Sub-Millimeter Heterodyne Focal-Plane Arrays for High-Resolution Astronomical Spectroscopy

Paul F. Goldsmith

Jet Propulsion Laboratory
California Institute of Technology
Pasadena CA 91109 USA
E-mail: paul.f.goldsmith@jpl.nasa.gov

1. Introduction

Spectral lines are vital tools for astronomy, particularly for studying the interstellar medium, which is widely distributed throughout the volume of our Milky Way and of other galaxies. Broadband emissions, including synchrotron, free-free, and thermal dust emissions give astronomers important information. However, they do not give information about the motions of, for example, interstellar clouds, the filamentary structures found within them, star-forming dense cores, and photon-dominated regions energized by massive young stars. For study of the interstellar medium, spectral lines at sub-millimeter wavelengths are particularly important, for two reasons. First, they offer the unique ability to observe a variety of important molecules, atoms, and ions, which are the most important gas coolants (fine-structure lines of ionized and neutral carbon, neutral oxygen), probes of physical conditions (high-J transitions of CO, HF, fine-structure lines of ionized nitrogen), and of obvious biogenic importance (H_2O). In addition, high-resolution observations of spectral lines offer the unique ability to disentangle the complex motions within these regions and, in some cases, to determine their arrangement along the line of sight. To accomplish this, spectral resolution high enough to resolve the spectral lines of interest is required. We can measure the resolution of the spectrometer in terms of its resolution, $R = f/\delta f$, where f is the rest frequency of the line, and δf is the frequency resolution of the spectrometer. More-active sources can be advantageously studied with $R = 3\times10^5$, while more quiescent sources require R as high as 10^7 .

At optical and infrared wavelengths, such resolutions can be achieved by diffraction gratings and Fabry-Perot interferometers. At sub-millimeter (or far-infrared) wavelengths, such approaches are significantly limited by diffractions, and they have not been able to reach such high resolution. Heterodyne systems – for which frequency resolution is generally not a limitation, except to the extent that there is a trade-off against signal-to-noise ratio (SNR) once the lines are resolved – have provided velocity-resolved spectroscopic information that in the past decade has transformed our understanding of the interstellar medium. The interstellar medium is extended over angular scales of many degrees, but has structure on scales as fine as have been accessible. To gain a complete picture of its structure thus requires extensive spectral-line images. Building up such a three-dimensional (two angular and one frequency) image one spectrum at a time is obviously time consuming. The development of arrays of heterodyne receivers has been driven by the need to make more-effective use of valuable observing time. Such a heterodyne focal-plane array (HPFA), employed in the focal plane of a large telescope, can increase the data rate by a factor equal to the number of elements in the array, and offers additional benefits in terms of calibration and data uniformity.

This paper offers a review of sub-millimeter heterodyne focal-plane arrays, and a selection of some of the recent results that have been obtained. Progress has been so rapid that it cannot be complete, but I hope it will illustrate some of the most important developments. Complementary information can be found in two earlier reviews [1, 2] that also cover longer-wavelength systems, and discuss some topics in more detail than possible here. I omit discussion of system aspects that are essentially the same for heterodyne focal-plane arrays as for single-element receivers, such as calibration. I will indicate some future technological areas that are currently being developed to improve the capability of future heterodyne focal-plane arrays.

2. Coherent Arrays and Focal-Plane Field Sampling

The heterodyne receivers that are being considered here are coherent systems, meaning that they have an output the phase of which is linearly related to that of the input electric field (whether or not we utilize the phase information). This is in contrast to an incoherent system, which has an output proportional to the power input. A

coherent receiver system, whether a heterodyne (mixer) system or an amplifier-based system, relies on a signal-processing device that is on the order of or smaller than the wavelength of the input signal. To efficiently transfer energy to the device from the input electric-field distribution produced by the telescope requires transforming the telescope focal-plane distribution, which is much larger than a wavelength in extent, to the much smaller signal-processing device. The latter is generally constructed in a single-mode propagation system, such as rectangular waveguide or microstrip, so that the transformer can also be thought of as a free-space-to-guided-wave transition.

A sub-millimeter transformer can be a feed horn, as widely used at cm and mm wavelengths, or a more optically-inspired transformer, consisting of an antenna combined with a lens. The wide range of wavelengths at which these ideas have been developed has resulted in those coming from shorter wavelengths using the term *telescope*, while those familiar with longer wavelengths generally refer to the generally parabolic radiation collector as an *antenna.* I shall use the terms interchangeably in this paper. I will also take the liberty of referring to some review articles on quasioptics and Gaussian beam propagation in which extensive reference lists to original research articles can be found.

We can analyze the coupling in one of two ways. The first is to calculate the electric-field distribution in the telescope focal plane produced by a source. For a point source producing a plane wave in the aperture of the telescope, this distribution is the Airy pattern [3, 4]. The coupling of this electric-field distribution to the field distribution of the feed horn or transformer yields the coupling. Of course, we can vary the parameters of the transformer to optimize the coupling for a given telescope operating at a given wavelength. However, it is often more effective to take advantage of the reciprocity theorem [5, 6], and to consider the signal-processing device as radiating a signal that is processed by the transformer to produce an electric-field distribution in the telescope's focal plane. From this distribution, we calculate the electric-field distribution in the aperture of the telescope, and from this we calculate the coupling to a plane wave. We can also calculate the far-field radiation pattern of the antenna, which enables understanding of how it will operate when observing an extended source. These issues have been analyzed in some detail in a variety of books and articles [6-8].

2.1 Fundamental Gaussian-Beam-Mode Modeling

While precise calculations do require knowledge of the detailed electric-field distribution in a transformer such as a feed horn, it is a fortunate simplification that many of the most important types of transformers can be accurately modeled in terms of having a fundamental-mode Gaussian electric-field distribution. This was examined in detail initially for corrugated feed horns, which are widely used at centimeter and millimeter wavelengths [9, 10]. However, other types of feed horns, including diagonal [11] and smooth-walled spline-profile feed horns, widely used at sub-millimeter wavelengths, can be treated in a similar fashion with good results, as well [12-15].

The fundamental Gaussian-beam mode has an electric-field distribution perpendicular to the axis of propagation given by

$$E(r)/E(0) = \exp\left[-(r/w)^2\right], \qquad (1)$$

where r is the distance from the axis of propagation, w is the beam's radius, and the electric field can have any polarization state. The field distribution can be normalized to the total power in the Gaussian beam, which is preserved as long as there is no truncation. The minimum beam radius is called the beam's waist radius, or simply the waist radius, and is denoted w_0. The beam's waist radius is located at the beam's waist, and increases in well-known fashion [16, 17] as a function of z, the distance from the waist:

$$w(z) = w_0\left[1+(z/z_c)^2\right]^{0.5}, \qquad (2)$$

where z_c is the confocal distance, given by

$$z_c = \pi w_0^2/\lambda\,. \qquad (3)$$

In the far field ($z \gg z_c$), the beam's radius grows linearly with z. From Equation (2), we find

$$w(z) = \lambda z/\pi w_0\,,\ (z \gg z_c)\,. \qquad (4)$$

2.2 Minimum Element Separation

To avoid truncation, an aperture located at position z' should have a diameter $D \geq 4w(z')$. From Equation (1), we see that $r' = 2w(z')$ gives an electric field equal to 0.018 of the on-axis value, corresponding to a relative power density equal to 3.35×10^{-4}, or -34.7 dB. This is sufficiently small to ensure that the fundamental Gaussian-beam mode can propagate essentially unperturbed. A very important constraint on coherent focal-plane-array systems is that high-quality transformers have $D \geq 3w_0$. The numerical factor here comes from least-squares fitting the fundamental mode to the actual field distribution, as described in [18]. Such transducers cannot be packed together with spacing significantly less than this.

The required value of the beam's waist radius is determined by the required illumination of the telescope's aperture. We can think of almost any telescope design as being equivalent to a focusing element (e.g., an antenna's main reflector) of diameter D_M and effective focal length f_E [6-8]. The focusing element is in the far field of the illuminating Gaussian beam's waist, which itself is near the focal point of the telescope. The relative power density at the telescope's edge is given by

$$P_{Edge} = \exp\left\{-2\left[D_M/2w(f_E)\right]^2\right\}. \quad (5)$$

The edge taper, T_E, is the logarithm of the inverse of P_{Edge} and more commonly one employs

$$T_E[\text{dB}] = 10\log_{10}(T_E)$$

$$= 10\log_{10}\exp\left\{2\left[D_M/2w(f_E)\right]^2\right\}. \quad (6)$$

Using this with Equation (3) gives us the convenient relationship [18]

$$w_0 = 0.216T_E[\text{dB}]^{0.5}(f_E/D_M)\lambda. \quad (7)$$

The choice of the optimum value of the edge taper depends on a variety of factors, including whether you want to maximize the aperture efficiency or reduce the spillover, as well as the size of any central blockage. The value chosen, together with the telescope's focal ratio, f_E/D_M, and the wavelength then determine the required radius of the beam waist (in one particular case, the size of the feed horn). The maximum aperture efficiency for an unblocked circular aperture is 0.815, which occurs for $D_M/2w(f_E) = 1.12$ or $T_E = 10.9$ dB [5]. This gives us the characteristic value for the beam's waist radius,

$$w_0 = 0.71(f_E/D_M)\lambda, \quad (8)$$

which in turn demands a minimum feed-element spacing that is three times this value, $X_{EL} = 2.14(f_E/D_M)\lambda$. The minimum spacing of elements of an array in the telescope's focal plane is thus not $0.5(f_E/D_M)\lambda$ as favored for some types of incoherent arrays, nor the dimensionally-derived $\sim(f_E/D_M)\lambda$, but over twice the latter value.

An unblocked circular antenna with a 10.9 dB edge taper has a FWHM beamwidth of $\Delta\Theta_{FWHM} = 1.17\lambda/D_M$ [19]. For a large focal ratio, the size in the focal plane corresponding to the FHWM beamwidth is just f_E times the angular size, or $\Delta X_{FWHM} = 1.17 f_E\lambda/D$. Comparing this with the spacing of the feed elements given above gives us

$$\Delta X_{EL} = 1.83\Delta X_{FWHM}. \quad (9)$$

The minimum transformer/array element spacing of any coherent system that efficiently illuminates the antenna corresponds to an angular spacing on the sky equal to almost twice the FWHM antenna beamwidth. Taking Equation (9) as a lower limit, and allowing for some gap between elements (for, e.g., feed-horn walls or lens mounting), the effective constraint is

$$\Delta\Theta_{EL} \geq 2\Delta\Theta_{FWHM}. \quad (10)$$

The pattern of the beams of any such array on the sky will thus leave a large fraction of solid angle unsampled, and *the beam spacing on the sky is at least twice the FWHM beamwidth*, as is shown in Figure 1. This obviously has a

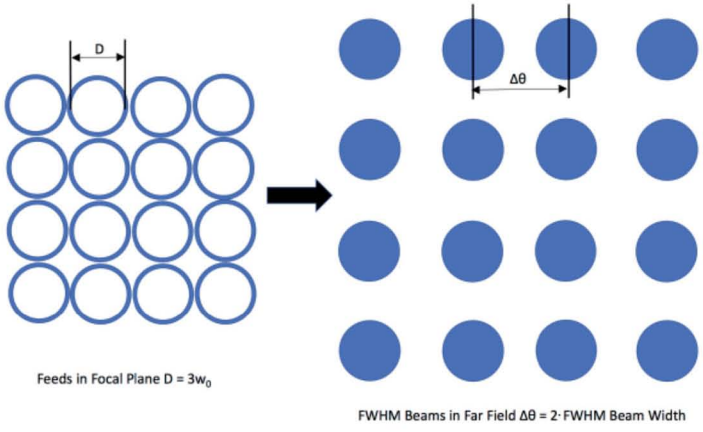

Figure 1. (left) A schematic of transformer apertures (e.g., feed horns) in a square configuration in the telescope focal plane. (right) The corresponding far-field beam patterns. The filled circles represent the FWHM beam size, which is approximately twice the full width to half maximum beam width, as given by Equation (10).

large impact on the observing strategy required to obtain fully-sampled images with coherent focal-plane-array systems.

2.3 Heterodyne Focal-Plane-Array Geometry

In sub-millimeter heterodyne focal-plane arrays implemented to date, only two geometries have been employed, and these are the same geometries as have been used at longer wavelengths. They are a square grid and a hexagonal grid of array elements. While the minimum elements and beam spacing are the same, the filling factor is higher for the hexagonal grid: the focal-plane area filling factors with no gaps for these are 0.079 for the square array and 0.091 for the hexagonal array. The hexagonal grid array thus has a slightly higher density of beams on the sky, and is more efficient for small sources (of a size between that of the beam and the footprint of the array). The square-grid array offers advantages in terms of ease of assembly of components into a modest number of array elements in a row, from which a two-dimensional array can be assembled. The seven-element CHAMP+ [20] and upGREAT [21, 22] are hexagonal-grid arrays, while the 16-element HARP [23] and 64-element SuperCam arrays [24,25] are square-grid arrays.

Until very recently, the numbers of elements in heterodyne focal-plane arrays have been so small that there was really no issue with the ability to efficiently couple energy from the telescope to an element in the array: telescope aberrations resulting in non-ideal electric-field distributions in the focal plane (or distorted far-field patterns, thinking reciprocally as introduced above) were not a serious issue. However, with increased capabilities, the number of pixels has increased, and telescope-imposed constraints have to be considered. One of the most straightforward is the limitation on the overall diameter of the beam that will fit through the telescope's optics. This is exacerbated by the relatively large focal ratio employed at Nasmyth or other focal positions that avoid motion in elevation. The limit can be the tertiary or a subsequent element, or the clear diameter through the elevation bearings. The secondary focal ratio, $f_E/D_M = 13.8$, together with limited elevation-bearing clearance on the Heinrich Hertz sub-millimeter telescope, required the addition of significant re-imaging optics for SuperCam operating at 345 GHz [24].

The Nasmyth focal ratio for SOFIA is 19.7, and $f_E = 49141$ mm [26], corresponding to a plate scale of 0.24 mm per arcsecond. At a wavelength of 0.158 mm (the fine-structure line frequency of C+), an optimal feed will have a waist radius equal to 2.2 mm, and an element diameter of ~ 6.6 mm. Allowing for a somewhat larger spacing, the diagonal size of a 10 × 10 element array is the maximum that can fit through the Nasmyth tube of diameter ~ 114 mm. Direct illumination of the SOFIA telescope would lead to prohibitively long feed horns with excessive loss. The solution is to re-image the telescope's focal plane to allow physically smaller waist and feed-horn sizes and beam spacings.

This is really part of a bigger issue, which is that as the wavelength decreases, so does the aperture size of the transducers (coupling devices) in the array, and thus the area available per pixel. While the actual size of the active mixer (superconductor-insulator-superconductor, HEB) or amplifier (MMIC) employed is extremely small – and to some degree, diminishes in proportion to the wavelength – the size of the connectors and bolts to hold pieces together cannot readily be reduced past a certain point. There thus has to be a change in the approach employed at some wavelength, which essentially involves a larger number of array elements in a single housing, possibly with IF amplifiers to avoid connectors. This does lead to concerns about device yield and reliability, testing, and replacement of individual components, all of which have to be addressed at a systems level for future large-format sub-millimeter heterodyne focal-plane arrays.

2.4 Free-Space-to-Guided-Wave Transformer Elements for HPFAs

The transformers (free-space-to-guided-wave transitions) used in arrays are generally just the same designs as used in a single-element receiver. The challenge is to pack them together as closely to the minimum spacing as possible. At the same time, system issues arise, including actual fabrication and assembly procedures, and servicing the signal-processing elements. The upGREAT array, operating on NASA's SOFIA observatory, uses seven individual mixers in a hexagon-plus-central-element configuration [22]. Each element employs an electroformed smooth-walled spline feed horn. With the chosen telescope illumination, the spacing of beams on the sky is 2.2 FWHM beamwidths [21]. While millimeter- and longer-wavelength arrays have generally employed individual feed horns (possibly modified to allow closer-than-standard spacing [27]), the smaller size characteristic of sub-millimeter arrays has led designers to integrate transformers into groups. In the case of the SuperCam 345 GHz array, eight elements, each with a diagonal horn, are machined as a unit, and eight such linear arrays are assembled to form the final 64-element array [24]. In order to minimize cost and simplify assembly and alignment, direct machining of multiple feed horns in a single block is attractive, particular when combined with multi-flare angle horns, which can be very efficient [12-15]. One such realization for 1.3 mm operation with 37 elements was described in [28].

This approach is increasingly attractive as the wavelength decreases, although machining tolerances become a concern even while the overall physical dimensions of an array with a given number of elements decreases. Recent work at JPL resulted in a 16-element array for 1.9 THz employing hot-electron bolometer mixers

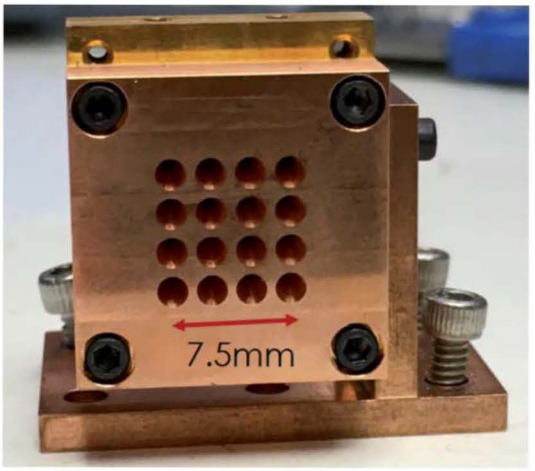

Figure 2. A 16-element 1.9 THz mixer array with smooth-walled spline feed horns in a square grid configuration. The block, including circular-to-rectangular waveguide transitions and pockets to hold the hot-electron-bolometer mixers, was directly machined from copper (photograph courtesy of J. Kawamura, JPL; see [29]).

and drilled profiled feed horns. The element spacing was 2.5 mm and the feed-horn diameter was 2.0 mm. There did not appear to be any problem from the point of view of fabrication in reducing the spacing-wall thickness to ~ 0.1 mm, which would reduce the spacing to 2.1 mm. As seen in Figure 2, direct drilling into a copper block combined good thermal properties with simplicity in fabrication [29, 30]. A circular-to-rectangular waveguide transition was machined for each element, and the back side of the block was machined to accept the hot-electron bolometer mixers, fabricated on small silicon substrates. The 16-element unit was completed by a back plate that also functioned as a back-short for each waveguide.

Free-space-to-guided-wave transformers, incorporating a planar antenna combined with a lens of approximately hemispherical shape, have been extensively used in single-element sub-millimeter heterodyne systems [31]. Recent work has taken up this approach, and currently-available powerful electromagnetic modeling allows optimization, with results at 545 GHz showing good agreement with theory [32]. This approach is extendable to focal-plane arrays with modern silicon fabrication techniques, allowing impressive accuracy [33]. The packing efficiency (the ratio of the lens diameter to the waist radius and the lens center-to-center separation) of such an approach should be reasonably high, although this aspect of performance has not yet been emphasized.

2.5 HFPA Configuration and Imaging

As discussed earlier, the minimum beam spacing on the sky of a reasonable telescope feed by an array with essentially close-packed elements is twice the FWHM beamwidth. Most of the sources being observed using sub-millimeter spectral lines are extended beyond the footprint of the array on the sky, and a spectral-line image from a heterodyne focal-plane array should ideally have pixels separated by the Nyquist-sampling interval ($\Delta\Theta_{PIXEL} = \lambda/2D$ for a telescope of diameter D) in both dimensions. To achieve this, motion of the array beams on the sky is necessary. This can be implemented by scanning the entire telescope or, to a limited extent, by the motion of an optical element between the telescope's primary and the receiver. Half-beam sampling ($\Delta\Theta = \Delta\Theta_{FWHM}/2$), somewhat coarser than Nyquist sampling, is often a compromise to reduce the required observing time.

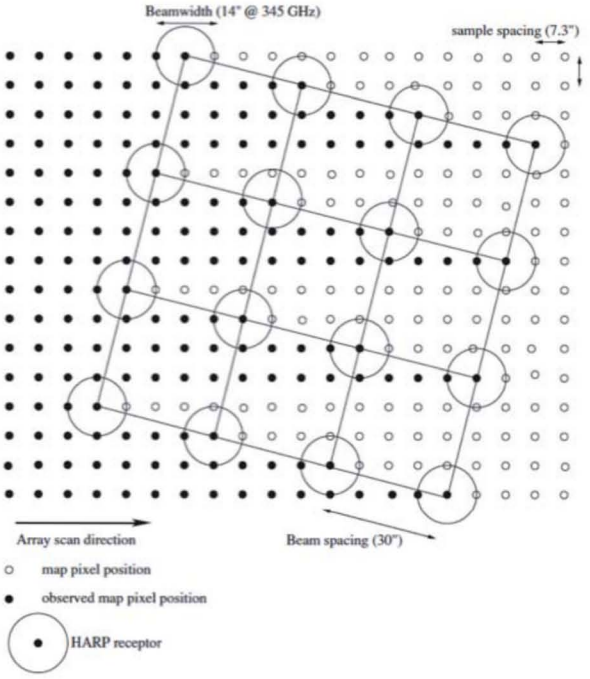

Figure 3. The rotation of a square array by ~14.5° to achieve half-FWHM beamwidth spacing perpendicular to the scan direction. The illustration is for the 16-elment HARP array on the JCMT [23], but is applicable to any square array with ≥16 elements.

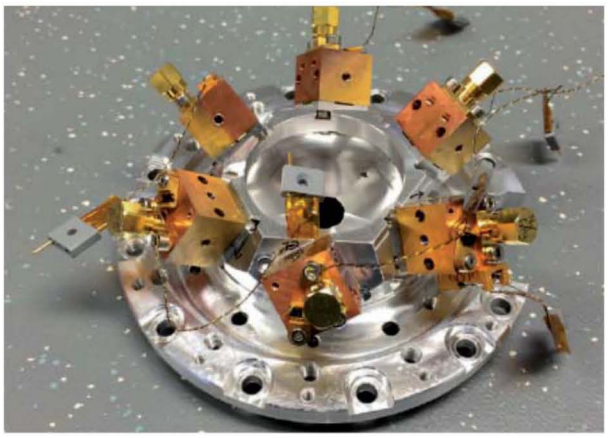

Figure 4. Six of the seven 2 THz mixers in a filled hexagon (6+1) configuration, on mounting structure used in the upGREAT LFA array. The central seventh element was independently mounted. The beams from the smooth-walled spline-profile feed horns were brought together in a centrally-mounted arrangement of parabolic mirrors (from [21]).

With a filled (6+1) hexagonal array, choosing the scanning direction to be at an angle of 19.1° relative to the hexagon's vertices results in the seven beams being equally spaced perpendicular to the scan direction. The beam spacing perpendicular to the scan direction is very close to one-third of the beam spacing on the sky, and approximately two-thirds of the FWHM beam size. This has been utilized for some time by arrays having this geometry [18, 20]. The resulting image is still under-sampled in the direction perpendicular to the scan direction, which can be remedied by a second scan offset by one beamwidth, giving approximately Nyquist sampling perpendicular to the scan direction. The outputs from each element have to be integrated for some finite period, enlarging the beam size somewhat along the scan direction, but samples can still be taken at sufficiently short intervals that the resulting image is properly sampled.

For a nine-element square array, rotation by 14.04° relative to the scan direction produces equally spaced beams with one-third or $2\Delta\Theta_{FWHM}/3$ spacing [34]. (The rotation angle is given as 14.48° in this reference). For a 16-element square array, rotation by 14.48° relative to the scan direction results in a spacing of beams perpendicular to the scan direction of one-quarter of the beam spacing, or close to $\Delta\Theta_{FWHM}/2$, which is extremely helpful in making well-sampled maps [23]. The configuration for a 16-element square array is illustrated in Figure 3. This general approach to scanning can be advantageously applied to square arrays with 16 or more pixels, giving Nyquist sampling perpendicular to the scan direction with a single scan for $N_{element} \geq 25$, leading to highly efficient imaging.

Figure 4 shows six of the seven 2 THz mixers of the upGREAT array utilizing a filled hexagon (6+1) configuration [21, 22]. This system has been extremely successful in producing high-spectral-resolution spectra and images at ~1.46 THz, 1.9 THz, and 4.75 THz, the frequencies of the fine-structure lines of the key constituents of the interstellar medium N^+, C^+, and O^0, respectively. The hexagonal geometry does not appear to be particularly valuable for larger arrays, which are easier to fabricate in a Cartesian geometry, and for which alignment issues may be much simplified. For almost any array configuration, a scanning strategy can be developed that minimizes the beam separation perpendicular to the scan direction. An important practical consideration is that different elements may well have different sensitivities, and having a one-to-one correspondence between a pixel in the image and an element in the array may not be optimum.

An on-the-fly mapping strategy that has each pixel on the sky observed by multiple elements of the array may result in more uniform noise and better calibration, even though more independent scans are required than the minimum-beam-separation approach. Scanning parallel to an array axis results in a high redundancy in the sense of a given map pixel being observed by multiple array elements. The integration time per element per pixel must be reduced, since for each pixel, data from multiple elements will be combined. A more-rapid scan speed is thus required. For very large maps, there is in the end no advantage in time between scanning with a "special" angle to get the best possible sampling with a single scan, and repeating the map made with gaps between the strips on the sky with small offsets to achieve the desired sampling. For fast sampling with many-element arrays and spectrometers with many channels, the data rate may become a problem, however.

3. Mixer Elements for HFPAs

Early sub-millimeter receivers employed Schottky diode mixers, and at least one focal-plane array (operating in the 3 mm wavelength range [35]) used this type of down-converter. By the time that people were seriously considering heterodyne focal-plane arrays, these had been supplanted by two more-sensitive technologies, the superconductor-insulator-superconductor (SIS) mixer and the hot-electron bolometer (HEB) mixer. Each of these has had a wealth of articles describing advances in the state of the art. Including even a representative sample of these is outside the scope of this article focusing on focal-plane arrays. Moreover, each of the articles cited here about a particular array includes a discussion of the mixer employed. I will thus give only a very brief overview of general characteristics, together with a limited selection of references.

Unless special efforts are made, mixers respond to two frequency bands that are offset from the frequency of the local oscillator by an amount equal to the frequency of the IF amplifier. The band with frequency greater than that of the local oscillator is called the upper sideband (USB), and that with frequency lower than the local oscillator is referred to as the lower sideband (LSB). Without such efforts (e.g., phasing circuits in RF and IF, which are well-

known from millimeter-wave experience, or appropriate setting of waveguide back-short at a large distance from the nonlinear element to differentiate between two sidebands), we have a double-sideband mixer. A mixer can be designed to down-convert only a single sideband (single-sideband or SSB mixer), or, using the phasing approach, can have separate outputs for the upper and lower sidebands (2SB mixer). If the mixer is sensitive to both sidebands, a single sideband can still be selected by the optics preceding the mixer, as discussed in Section 4.3.

3.1 SIS Mixers

The principles behind the operation of superconductor-insulator-superconductor mixers and limits on their performance were discussed thoroughly in early articles that clear established the potential for these devices to offer near-quantum-noise-limited performance [36, 37, and references therein]. The *I-V* characteristic of the tunnel junction has an extremely strong nonlinearity, and the presence of radiation induces photon-assisted tunneling steps onto the dc *I-V* curve. In principle, the result is that each incident photon can generate a carrier flowing through the junction, which leads to the possibility of quantum-noise-limited performance. Initial development of superconductor-insulator-superconductor mixers occurred at millimeter wavelengths (e.g., frequency ~100 GHz), since lower frequencies had transistor amplifiers, parametric amplifiers, and masers offering performance often limited by other factors, such as atmospheric and ground pickup.

The astronomical interest in millimeter wavelengths had been growing at a rapid pace since the 1970's, driven to a large degree by the discovery of a stupendous variety of molecules in interstellar clouds. The state of the art for low-noise receivers was soon almost entirely defined by superconductor-insulator-superconductor mixers at frequencies up to many hundred GHz, developed for use on a variety of ground-based radio telescopes [37-39]. The Atacama Large Millimeter/Submillimeter Array (ALMA), which until now has relied almost entirely on superconductor-insulator-superconductor receivers [40], provided additional major impetus for development of superconductor-insulator-superconductor receivers up to 1000 GHz. The Herschel Space Observatory offered complete freedom from atmospheric absorption, which is a major impediment to low-noise systems even from mountain sites. The Heterodyne Instrument for the Far-Infrared (HIFI) employs dual-polarization superconductor-insulator-superconductor receivers in five bands, extending from 480 GHz to 1250 GHz [41], with the upper frequency limit set by the bandgap of the Nb/Nb-alloy junction employed.

Incorporating superconductor-insulator-superconductor mixers into focal-plane arrays at millimeter and sub-millimeter wavelengths has been demonstrated in a variety of configurations over a wide range of frequencies (e.g., [20, 22, 24, 42, 43]). Challenges arise from the number of lines required for controlling the mixer bias, the current of the magnet (required to suppress Josephson tunneling of Cooper pairs), and the IF output. These have been overcome for arrays up to 64 pixels [24, 25], which achieved just over $2\Delta\Theta_{FWHM}$ spacing on the sky, despite the number and variety of connections to each element required. Figure 5 gives two views of an eight-element column of this array, with the upper view including the electromagnets used for Josephson-current suppression. The aperture size of the diagonal horns employed was sufficient to allow only nominal gaps between the corners of feed horns in adjacent columns, giving close-to-minimum spacing of the beams on the sky. This challenge becomes greater at shorter wavelengths, where the transformer or feed-horn size for a given focal ratio decreases, demanding closer packing of the array elements to achieve the minimum $2\Delta\Theta_{FWHM}$ beam spacing on the sky.

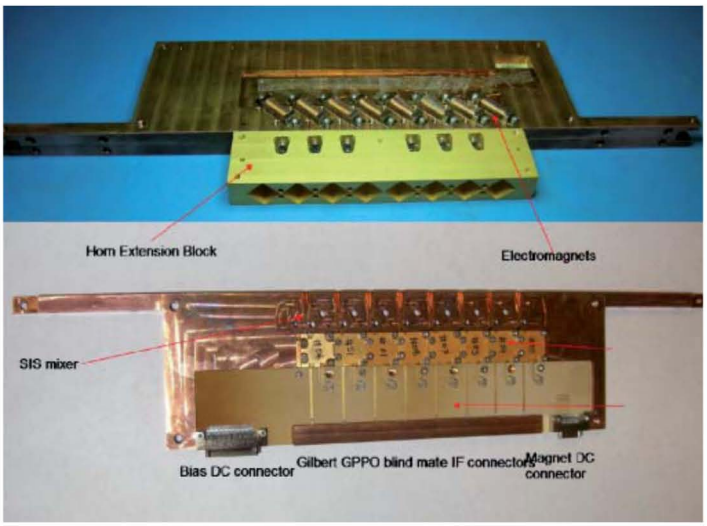

Figure 5. A view of one eight-element column of SuperCam elements. The upper view shows the electromagnets used to suppress the Josephson current in the superconductor-insulator-superconductor mixers, and the diagonal feed horns. The spacing of adjacent columns was just greater than the diagonal dimension of the feed horns, and was greater than the size of the electromagnets, allowing nearly minimum $2\Delta\Theta_{FWHM}$ beam spacing on the sky (from [24]).

3.2 HEB Mixers

In a material for which the electrons are only weakly coupled to the lattice, radiation can be absorbed by the electron gas, which achieves a well-defined temperature higher than that of the lattice temperature. Such a hot electron gas can function as a bolometer with a very short time constant. Such a device is appropriately called a hot-electron bolometer. If a locally produced signal of appropriate magnitude is introduced along with a signal at a different frequency, the nonlinear response of the electrons results in mixing action, with an IF signal at the difference of the two signals being produced. This was the basis for the hot-electron bolometer mixer, employing bulk InSb cooled to 4K, designed for astronomical observations in the 90 GHz to 140 GHz range [44]. This type of hot-electron bolometer mixer was used for observations at 230 GHz [45] and 490 GHz [46], illustrating the independence of the effect on input frequency. The coupling between the electrons and lattice for this material and configuration limited the IF bandwidth to ~ 2 MHz, making it necessary to tune the local oscillator even for spectral-line observations. The rapid development of low-noise cooled Schottky barrier diode mixers with multi-octave IF bandwidths and modest LO power requirements (e.g., [47]) left limited scope for the use of the InSb hot-electron bolometer mixer technology in astronomy.

Interest in hot-electron bolometer mixers revived almost 20 years after the work on InSb, with the realization that the superconductor NbN, biased near the resistive state, exhibits hot-electron effects [48], and in that if fabricated in the form of microbridges, the response time can be made rapid enough to have GHz IF bandwidths. The response time is determined by electron-phonon coupling and rapid phonon escape (denoted "phonon-cooled" [49]), or by rapid diffusion of the hot electrons to a heat sink formed at the ends of the microbridge (denoted "diffusion-cooled" [50]). This device has many attractive features [51], and was rapidly adopted for systems at frequencies above those where superconductor-insulator-superconductor mixers could operate. Some examples of relatively early systems spanning 692 GHz to 5250 GHz were given in [52-55].

Continued development of hot-electron bolometer mixers has resulted in noise temperatures in the range 800 K to 1000 K (DSB) at all sub-millimeter wavelengths (see above references and [56]). The geometry of the small-area microbridge between two much larger conductors is amenable to connection to either microstrip for coupling to waveguide and from there to feed horns [53, 54, 57], or to planar antennas [55, 56]. The noise temperatures corresponded to ~ 20 times the quantum limit at 1000 GHz, and ~ 4 times at 5000 GHz. There is thus still room for considerable improvement, especially at longer sub-millimeter wavelengths.

The local oscillator power absorbed by the hot-electron bolometer itself is typically 100 nW to 300 nW, but the LO power incident on the mixer itself needs to be up to an order of magnitude greater [53, 57], so that ~ 1 μW per element is required for an array. A modest number of array elements can be pumped by frequency-multiplied sources at frequencies up to ~ 3 THz at the present time, and by quantum-cascade lasers at higher frequencies (discussed further in Section 4).

The electron gas relaxation time limits the IF bandwidth, so that while bandwidths up to 4 GHz have been reported, the receiver noise temperature can easily be a factor of two higher at the upper limit of the IF than it is below $f_{IF} = 1$ GHz [55]. The restricted instantaneous bandwidth of hot-electron bolometer mixers is one impetus behind the search for new materials that might offer faster relaxation times and thus greater IF bandwidth. One such material is magnesium diboride (MgB_2) [58, 59]. While the stronger rapid electron-phonon interaction should allow significantly increased IF bandwidths, reported results still showed very significant increases in noise temperature when comparing IF frequencies of a few GHz to the vicinity of 10 GHz [60, 61]. Another virtue of MgB_2 is its relatively high superconducting-transition temperature, $T_c = 39$ K [61], which in principle can allow operation at significantly higher physical temperatures compared to, e.g., NbN. A possible issue, especially for arrays, is that the local oscillator power required will be larger than for devices having lower T_c.

Incorporation of hot-electron bolometer mixers into arrays is relatively straightforward, but there are some challenges. There are no magnets required to suppress Josephson currents as for superconductor-insulator-superconductor mixers, but cabling is still a challenge. One extra demand of hot-electron bolometer mixers is that they are relatively sensitive to LO power, unlike Schottky or superconductor-insulator-superconductor mixers that operate well as long as the LO power is above a certain threshold. Measurements of mixers designed for Herschel showed that a change of 50% in the local oscillator power from its optimum value increased the mixer noise by a factor of two [62]. This indicates that (1) the LO power level must be carefully controlled to ensure receiver stability, and (2) device fabrication and other variations mean that individual hot-electron bolometer mixer elements may require different LO power levels for optimum operation. The former applies for both single-element systems and arrays, while the second is significant only for arrays.

3.3 Possibilities for the Future

Superconductor-insulator-superconductor mixers are the favored down-converter element for HPFAs at longer sub-millimeter wavelengths, but are currently limited to ~ 1100 GHz by the superconducting bandgap. There is ongoing work to extend superconductor-insulator-superconductor technology to higher frequencies, where some of their advantages – notably, low noise (compared

to the quantum limit) and high instantaneous bandwidth – will be important. These may outweigh the system complexity engendered by having to employ a magnetic field to suppress the Josephson current in the devices. hot-electron bolometer mixers do not approach the quantum noise limit as closely as do superconductor-insulator-superconductor mixers, but their lower local-oscillator power requirement becomes particularly important if broadly tunable frequency-multiplied sources are employed, as contrasted to much higher power but difficult-to-tune quantum-cascade lasers. Finally, monolithic microwave integrated circuit (MMIC) amplifiers, which have achieved noise temperatures only a few times the quantum noise limit at 100 GHz [63, 64] are already being used in focal-plane arrays in this frequency range [27, 65]. InP high-electron-mobility transistor (HEMT) MMIC amplifiers are rapidly moving upwards in frequency, and have respectable but far from quantum-limited noise temperatures well into the sub-millimeter-wave region [66, 67]. These devices have several significant advantages from a systems engineering standpoint, especially for space missions. These include (1) the ability to work over a wide temperature range (~ 15 K to 300 K); (2) the noise temperature decreases and the gain increases with decreasing physical temperature, but without any hard requirement; (3) very large instantaneous bandwidth can be achieved, allowing simultaneous observation of multiple spectral lines; (4) the absence of sideband gain-ratio issues, which are a challenge for mixers or increase system complexity. How far their upper frequency limit will extend and how low a noise they can achieve will determine to what degree they can supplant mixers as the first element in sub-millimeter heterodyne focal-plane array receivers.

4. Array Optics and Local Oscillator Generation, Distribution, and Injection

Sub-millimeter arrays quite naturally make extensive use of free-space propagation, as loss in waveguide and other guided-wave media is excessively large for all the required functions to be implemented in such transmission media. As discussed in Section 2, the transverse dimensions of optical elements when measured in wavelengths dictate that diffraction will play a significant role, so that quasioptical propagation will determine beam growth and dictate the required size of different types of components (e.g., [8]). The articles describing the various sub-millimeter heterodyne focal-plane arrays that have been designed and built are the best source of information about adopted practices, and often themselves give references to more-basic articles. The actual active devices, whether mixers or amplifiers, are far, far smaller than a wavelength, so the optical system must couple to them via a free-space-to-guided-wave transformer, as discussed in Section 2.4.

The most important functions provided by the optical system include re-imaging of the array beams and local-oscillator injection. Optical single-sideband filtering and image rotation are employed in some systems, as discussed in the following sections.

4.1 Re-Imaging

Re-imaging the focal plane is required if the focal ratio of the telescope is not compatible with the capabilities

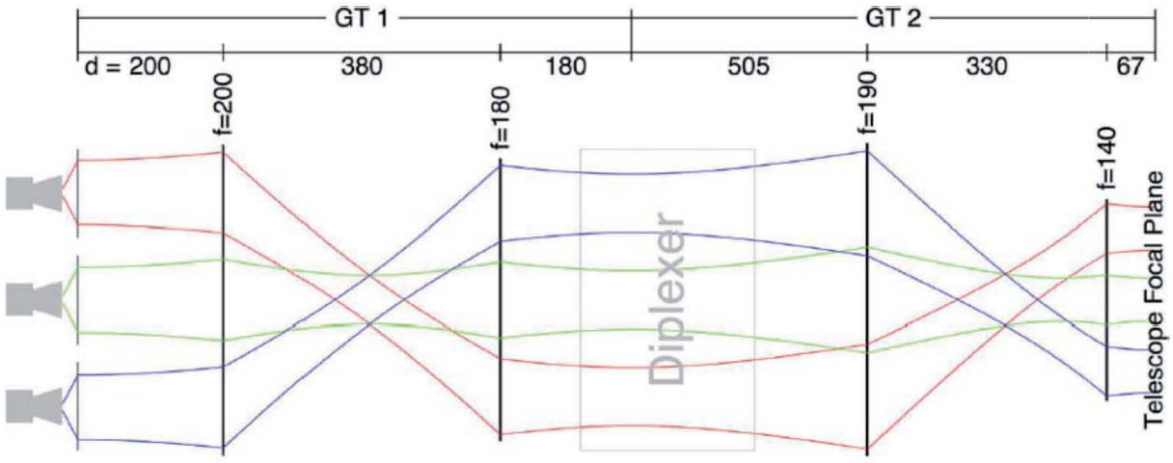

Figure 6. A schematic of the re-imaging optics used in the upGREAT receiver. The focusing elements (off-axis mirrors) are denoted by vertical black lines, labeled by their focal lengths and inter-element distances in mm. The combinations of pairs of focal lengths define the two Gaussian-beam telescopes, denoted GT 1 and GT 2 (from [21]).

of the transformers or feed horns coupling energy to the individual elements of the focal-plane array. For example, the SOFIA telescope's focal ratio is $f_E/D_M = 19.6$. For a 13 dB edge taper as used in the upGREAT system, from Equation (7), at the 158 μm wavelength of the ionized-carbon fine-structure line, then the beam's waist radius $w_0 = 2.4$ mm, and the nominal feed-horn diameter would be 7.2 mm. Such a horn would be difficult to construct, as it would need to either be extremely long, or to have a phase-correcting lens at its aperture. Instead, a quasioptical re-imaging system is far preferable. A schematic of the system described in detail for upGREAT from [21] is shown in Figure 6. In the figure, "GT" stands for Gaussian-beam telescope. This is a pair of focusing elements separated by the sum of their focal lengths, which offers frequency-independent transformation of the beam's waist radius. The first Gaussian-beam telescope transforms the waist of each beam in the telescope's focal plane to that required for the LO diplexer, and the second transforms the beams' waist radii to couple properly to the feed horns of the array.

Focusing elements can be either lenses or mirrors. Lenses have some advantages in terms of mechanical layout, but require surface treatment to control reflection loss. While mirrors are essentially free of absorptive loss, which is a factor for lenses, other considerations make the choice less than obvious. Off-axis optical elements produce cross polarization and beam distortion, which can be appreciable for large off-axis angles and divergent beams. The use of this type of focusing element thus does put constraints on the overall system layout [18]. Some materials, notably sapphire, have impressively low loss at cryogenic temperatures, and the application of dielectric-film antireflection coatings has been shown to be effective and reliable.

A variety of other considerations must be taken into account for optical design for sub-millimeter arrays. The diameter of a focusing element in a system propagating a single fundamental Gaussian-beam mode must be chosen to be at least four times the beam radius, w, at that element. This is in order to avoid beam truncation, which not only loses power from spillover, but results in higher-order modes due to the beam profile being less purely Gaussian. For an array, we have a number of well-separated beam waists in the telescope's focal plane, and in the plane in which the feed horns or other free-space-to-guided-wave transformers are located. In between, the beams significantly overlap, and the overall size of the array beams can be much less than the sum of the individual beams. This is seen nicely in Figure 6, where at the intermediate beam waist of each Gaussian beam telescope, the beams are almost entirely overlapping. These are the locations at which to put components of limited transverse dimensions, such as a Dewar window.

4.2 Local Oscillator Generation, Distribution, and Injection

The generation, distribution, and injection of the local oscillator (LO) into the mixer elements of a heterodyne focal-plane array can be entirely separate tasks, or they can be highly interrelated. Starting with the generation of the local oscillator, we have sources that oscillate themselves at the frequency of interest. As local oscillators, optically pumped lasers have largely been abandoned, due to their bulk and power consumption, and difference-frequency generation does not produce an adequate power level. The only widely-used photonic local-oscillator source – the niche for which, at the present time, is at shorter sub-millimeter wavelengths – is the quantum cascade laser (QCL) (see [68, 69] and references therein). These lasers depend on a cavity fabricated in the semiconductor material to set the frequency of oscillation, which gives good spectral purity. The quantum cascade laser's frequency can be somewhat tuned using the bias voltage and temperature. For astronomical spectroscopy, they can be frequency-locked [70] or phase-locked [71], but the frequency stability of the free-running quantum cascade laser may be sufficient that this complexity can be avoided.

Quantum cascade lasers have relatively high power (0.1 mW to 1 mW), which obviously makes pumping the elements of an array relatively straightforward by power division. Early quantum cascade lasers were handicapped for use as local oscillators due to highly non-Gaussian beam patterns and low coupling efficiency, but this has been improved [72]. At the present time, these devices must be operated at cryogenic (10 K to 77 K) temperatures, at which ≥ 1 W of power is dissipated. A complete sub-millimeter radiometer employing a quantum cascade laser was described in [73]. This quantum cascade laser included 21 lasers fabricated together, having frequencies spaced by 7.5 GHz, giving an overall tuning range of over 100 GHz around 4700 GHz.

The second widely-used approach for sub-millimeter local oscillators is frequency multiplication of a low-frequency oscillator. The fundamental oscillator can be at almost any frequency but is typically at 10 GHz to 40 GHz. Multiplication is by a cascade of multiplier stages, usually frequency doublers and frequency triplers. This approach was extensively used for the local-oscillator system of the Herschel HIFI instrument [41]. Cascaded multiplier chains are generally modestly tunable over a fractional bandwidth of $\pm 10\%$, but which is generally less than that of the mixers they are pumping. Since the total efficiency of the chain is quite low, the total RF power and the dc power dissipation can be an issue, especially for arrays. The efficiency generally decreases with increasing frequency, due to the increased number of cascaded multiplier stages required.

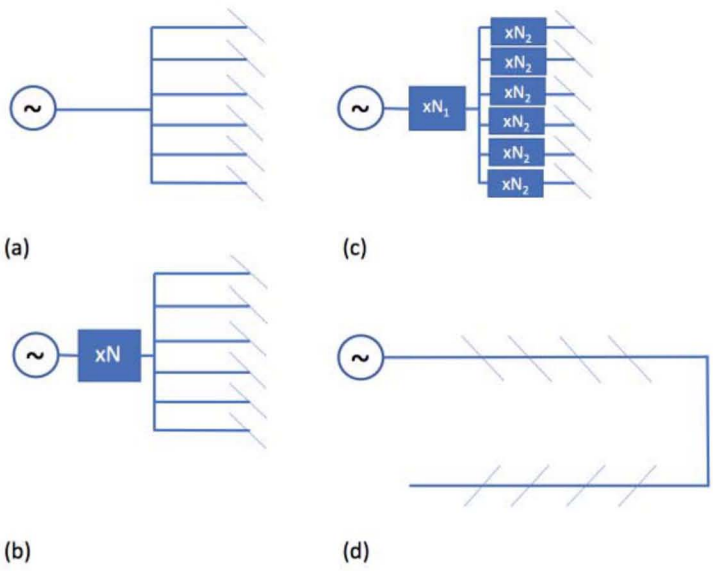

Figure 7. A schematic of different approaches for dividing the local oscillator among different elements of the HPFA. (a) A fundamental local oscillator (e.g., a quantum cascade laser) divided among different elements. The division can be carried out by quasioptical power-dividing grids or by a Fourier grating. The diagonal dashed lines represent the injection paths, which could be quasioptical dielectric beam splitters, interferometers, or (in principle) waveguide couplers. (b) The same approach but with a lower frequency source, multiplied by a factor *N* before division and coupling to the array mixers. (c) An approach in which the frequency multiplication is in part before power division, and in part after. (d) Series power division, in which a certain fraction of the local oscillator power is coupled from the main line to the individual mixers, in succession.

The performance of frequency-multiplier local-oscillator chains that have been reported include power outputs of ~1.5 mW at 850 GHz to 900 GHz [74], 35 μW at ~1500 GHz [75], and ~20 μW at ~1880 to 1940 GHz [76]. These numbers were all for multiplier-chain physical temperatures of 120 K, which did produce a 25% improvement in output power compared to ambient-temperature operation. These numbers should not even be taken as the current state-of-the art, as major increases in efficiency and output power are being made at the present time. However, the relatively limited output power relative to the requirements of hot-electron bolometer mixers at shorter sub-millimeter wavelengths indicates that only a limited number of elements can be pumped by a single frequency-multiplied local-oscillator source.

A commonly used component at microwave and millimeter wavelengths is the balanced mixer, in which two mixers are used together with appropriate phase shifts from hybrid power junctions to allow the local oscillator and signal from separate input ports to both couple to the mixers. This is generally referred to as a balanced mixer, inasmuch as the use of a pair of mixers, if properly balanced, can cancel out noise that may be present on the local oscillator. This has been successfully used at a frequency of 2.7 THz [77], giving noise performance comparable to that of the individual mixers. However, balanced mixers have not been used in any sub-millimeter array with published results. This is likely due to the increased complexity of high-precision waveguide machining, having two mixers, and the increased size resulting not only from two mixers and an RF hybrid, but from the necessarily relatively large IF hybrid, as well. However, with a nominal insertion loss of only 3 dB for the local oscillator, they do become increasingly attractive when local-oscillator power is limited.

For array systems at the present time, we thus have to consider how the local oscillator is divided among the array elements, and how it is injected into the individual mixers. Some different schemes for realizing this are shown in Figure 7. Figures 7a-7c illustrate different variations on parallel power division. In Figure 7a, we start from a fundamental source – most likely, a quantum cascade laser – and divide it among the array elements. The division can be carried out by waveguide power division, by quasioptical beamsplitters [8, 23], by a Fourier grating [78, 79], or by a collimating Fourier grating [80].

The power division is followed by coupling into the individual mixers of the array. This task is most commonly carried out either by a dielectric beamsplitter, or by an interferometer. The beamsplitter approach is very simple and broadband. However, it typically utilizes a 10 dB beamsplitter, meaning that only 10% of the available local oscillator power is used, while the rest is wasted (and must be absorbed in a beam dump). A direct consequence of the splitter is that 10% of the signal is wasted as well, which is generally judged to be an acceptable loss. The interferometer approach is most commonly based on a dual-beam interferometer [8, 18, 81]. This approach uses signal and local oscillator power much more efficiently, but at the price of much greater mechanical complexity (the system must in general be tunable) and optical constraints (each type of interferometer requires a minimum beam-waist radius to have low loss), as well as some limitation on the IF bandwidth, due to the characteristic response of the interferometer. For many-element focal-plane arrays, the difficulty of having the interferometer be properly tuned for all beams is an additional challenge, but one that should be possible to overcome by careful optical design.

Figure 7b shows the same approach, but with a frequency-multiplied source, which is not different in any fundamental way from Figure 7a. A waveguide power divider is followed a frequency-multiplied source [24]. With this configuration, a single dielectric beamsplitter could serve as the local-oscillator coupling element for all 64 mixers.

Figure 7c illustrates a variation in which there are active frequency multipliers both before and after the power division. All of the multiplier stages are in waveguide, as is the power division. The frequency at which the power division occurs is a tradeoff based on what power amplifiers are available at what frequencies. This approach has the advantage that the final multiplier stage has to deliver power sufficient to pump a single mixer, as compared to, e.g., Figure 7b, were all of the array mixers must be pumped by a single multiplier. It has a second major advantage in that the power output of each element of the local-oscillator array can be independently adjusted. This is particularly valuable for pumping hot-electron bolometer mixers, which as noted above are relatively demanding in terms of local-oscillator power in order to obtain optimum noise performance. The negative aspects of this approach are the large number of active components required, and the resulting total power dissipation. The various frequency-multiplication stages can be distributed between ambient temperature and cryogenic locations as dictated by constraints on cooling capacity. The final stage(s) could even be integrated with the individual mixers in the heterodyne focal-plane arrays.

Figure 7d illustrates a rather different approach, in which each in a series of couplers takes a certain fraction of the power flowing down the main line, and couples it to a mixer. This can be done using either waveguide [35] or quasioptical [23] propagation. If the coupling values are all the same, the mixers will systematically get different amounts of local-oscillator power. However, if the coupling values can be selected, the power made available to each mixer can be relatively uniform, and the overall efficiency of use of the local-oscillator power can be significantly higher than in the parallel power division configurations shown in Figures 7a through 7c.

4.3 Single-Sideband Filtering

Mixers made from a single nonlinear element (Schottky, superconductor-insulator-superconductor, or hot-electron bolometer) are typically sensitive to input frequencies both higher and lower than the local-oscillator frequency, within the two bands defined by the bandwidth of the IF system. These systems are thus referred to as double-sideband or DSB mixers. As discussed at the start of Section 3, a pair of such mixers can be combined, using two 90° hybrid junctions – one at RF and one at IF – and one RF in-phase power divider, to make a single sideband or SSB (also referred to as a sideband-separating or 2SB) mixer. In such devices, there are generally two IF output ports, one for the upper and one for the lower sideband [40, 82, 83]. This is in principle a great advantage for spectroscopy, as spectral lines may well be present in both sidebands. Having them separately available for analysis avoids overlaps and blending, as well as improving the situation for input noise-like signals common to both sidebands (e.g., atmospheric or telescope emission), which is folded from both RF sidebands into the single IF output by a double-sideband mixer, but kept separate by a single-sideband mixer.

The ratio of the response in the two sidebands is referred to as the sideband-gain ratio or the image-rejection ratio. It often does not significantly exceed 10 dB in real sub-millimeter mixers, likely due to manufacturing imperfections in the waveguide circuitry employed. In some situations it may be possible to correct for this by replacing the IF quadrature hybrid by a digital version that can have programmed phase shifts based on maximizing the sideband-gain ratio [84]. Since even spectral-line systems are generally calibrated using a blackbody source, this sideband-gain ratio is not readily measured. It can be determined by laboratory measurements with spectral-line sources, which can be quite tedious when large RF and IF bandwidths are involved. Astronomical observations of spectral-line-rich sources offer an important additional calibration tool [85]. This is especially important for space missions, where hands-on calibration cannot be used to verify post-launch operation including the sideband-gain ratio.

All of the above considerations apply to heterodyne focal-plane arrays as well, but to date, arrays have not utilized the single-sideband/2SB mixers discussed above. Rather, the same dual-beam quasioptical interferometers used for local-oscillator injection discussed above have been employed. The HERA array is a lone standout among the arrays included in Table 1, in that it achieves single-sideband operation by having the mixer back-short positioned to tune only a single sideband and, to a level of ~ 10 dB, suppress response in the opposite sideband [34]. Rather, the approach most widely adopted to achieve single-sideband operation is to employ double-sideband mixers and to select a single by means of a tunable quasioptical filter, e.g., [23].

4.4 Image Rotation

Inasmuch as almost every sub-millimeter telescope employs an azimuth-elevation mount, the image of a given field being tracked rotates as a function of time. For a single on-axis element, this produces only a rotation of the plane of polarization to which the array is sensitive, if linear polarization is employed. For an array, the direction of the beam corresponding to each element of the array changes with time. This can simply be ignored if large-scale relatively rapid mapping is the mode of observation. While the directions of the scan will change, the computer software can be written to compensate for this to ensure

Table 1. Sub-millimeter heterodyne arrays used for astronomical observations.

Array Name	Frequency (GHz)	$N_{element}$	Mixer Type	LO Injection	Image Rot.	SSB Filter	Telescope	Ref	Comments
HERA	220-260	9	SIS	WC	K	BT	IRAM 30 m	[32]	
CHAMP	460-490	16	SIS	FG+MPI		MPI	CSO 10 m	[91]	Also other telescopes
Pole STAR	810	4	SIS	ML+MPI			AST/RO 1.7 m	[92] [93]	
SMART	490/810	8/8	SIS	CFG+MPI	K		KOSMA 3 m	[94]	Dual band; NANTEN 4 m
Desert STAR	345	7	SIS	CFG+DBS			HHT 10 m	[95] [96]	
CHAMP+	670/860	7/7	SIS	CFG+MPI	RX	MPI	APEX 12 m	[20]	Dual Band
SuperCam	345	64	SIS	WPD+DBS			HHT 10 m	[24] [25]	Also APEX 12 m
HARP	345	16	SIS	ML+DBS	K	MZI	JCMT 15 m	[23] [97]	
upGREAT	2000/4700	14/7	HEB	CFG+WG	K		SOFIA 2.5 m	[21] [22]	Dual Band

Notes to Table 1

SIS Superconductor-insulator-superconductor
HEB Hot-electron bolometer
WC Waveguide coupler
FG Fourier grating
MPI Martin-Puplett interferometer
ML Meander line
CFG Collimating Fourier grating
DBS Dielectric slab beam splitter
WPD Waveguide power divider
WG Wire grid beam splitter
K K-mirror
RX Receiver rotated
BT Image rejection by back-short tuning
MZI Mach-Zender interferometer

that the images of individual "scan blocks" properly fit together. However, for longer integrations on a particular field, it is necessary to hold the rotation angle of the array fixed relative to the sky.

Some of the techniques that have been developed to achieve this are included in Table 1. A straightforward approach is to mechanically rotate the receiver. This may be undesirable or impractical, in which case the use of an optical "K mirror" is quite commonly used. In this configuration, the array of input beams goes through a series of reflections from a mirror on the axis of propagation of the array beams, but inclined to it. The beams then reflect from a second mirror off of the original axis, and with its normal perpendicular to the original axis of propagation. Finally, the beams reflect from a third inclined mirror that is on the beam axis. The inclinations of the two on-axis mirrors and the distance to the second mirror are arranged so that at the output of the K mirror, the array beams are traveling in their original direction and along their original axis of propagation. However, rotation of the off-axis mirror by angle Φ around the axis of propagation results in rotation of the array's pixels relative to their original orientation by angle 2Φ.

A K mirror is employed in almost half of the heterodyne focal-plane-array systems included in Table 1, and it is generally not a problematic aspect of the overall system. There is obviously some loss due to the three surface reflections (dependent on frequency [8]). The K mirror itself requires a rotary stage with a clear bore diameter at least as large as the combined cross section of all of the beams as they have propagated from their waists through the K mirror assembly. The axis of the K mirror must be accurately aligned with that of the incident array beams to avoid beam wander as the K mirror assembly is rotated.

4.5 Other

The optical system in sub-millimeter heterodyne focal-plane arrays necessarily links together a variety of components to carry out functions including those mentioned above. Since most of them are not different from those in single-element systems, we will not further discuss them here. One exception is the fact that for a heterodyne focal-plane-array system with independently fabricated and mounted pixels, it is necessary to verify the correct positioning and alignment of beams in the focal plane of the telescope to which the instrument will be mounted. At frequencies above 1000 GHz, this is not currently a measurement that is straightforward to make with, e.g., a near-field scanning system. This has led to development of special systems for this purpose: [86] describes one such system that has been effectively used with the upGREAT system on SOFIA.

5. IF Amplifiers and Other Cryogenic Considerations

Any mixer used for sub-millimeter astronomy will be cooled, most commonly to 15 K or 4 K. Along with the

down-converter stage, the first gain stage, the IF amplifier, is critical in determining the noise of the entire system. Of course, the exception is if the first stage is an amplifier, in which case down-conversion and further amplification are of diminished importance, due to the gain of the preceding stages.

When the first stage is a mixer, locating at least the first few stages of IF gain in close physical proximity to the mixer has the advantages of eliminating transmission-line loss and allowing larger IF bandwidths in light of possible impedance mismatch between the mixer IF output port and the IF amplifier input. This is particularly important as the RF frequency increases and the IF bandwidth required simply to accommodate the line width in a source such as the galactic center, with a Doppler width in excess of 300 km/s, reaches 5 GHz for an input frequency of 4700 GHz (corresponding to the important 63 μm fine-structure line of atomic oxygen). Integrating the IF amplifier with the mixer is an excellent approach. This was done for superconductor-insulator-superconductor mixers and MMIC amplifiers having ~ 32 dB gain in each of the elements of the SuperCam array [24]. One limitation that is not significant for single-element sub-millimeter receivers, but can be a problem for arrays with many elements, is dc power dissipation. The MMIC amplifiers described in [24] dissipated 6 mW each, which was acceptable in that system.

Current developments in SiGe amplifier technology indicate that much lower dc power dissipation should be achievable. An amplifier having a noise temperature of < 5 K and a gain > 27 dB over the 1.8 GH to 3.6 GHz frequency range at a 15 K physical temperature dissipated only 290 μW [87]. This is enabling technology for large sub-millimeter heterodyne focal-plane arrays. However, the challenges that remain include (1) achieving even broader bandwidths, preferably extending close to dc to maximally utilize the available IF bandwidth of hot-electron-bolometer mixers (discussed in Section 3.3); and (2) shrinking the footprint of the amplifiers to conform with the closer spacing required at shorter sub-millimeter wavelengths. 1.9 THz 16-element mixer array shown in Figure 2 (see [29]) had an element spacing of only 2.5 mm. However, a spacing of 5 mm is a plausible compromise, as feed horns with the aperture diameter match to a reasonably sized beam, while allowing more space for the mixers as well as for the IF amplifiers if integrated with the mixers.

The IF output from each array element has to be connected to subsequent amplifier and processing stages at ambient temperature. If there has been some gain before the ~ 300 K temperature gap needs to be crossed, low-thermal-conductance IF cables can be employed. Their additional loss at the IF frequency will have negligible impact on the overall system noise temperature. Other strategies include having additional gain at different temperatures, where the thermal load through the IF cables can be absorbed and not reach the mixers at the lowest temperature in the system, where the heat lift is the smallest. Having the very low-power first IF amplifier gain stage (or stages) integrated with the mixer simplifies the situation, but the thermal design of sub-millimeter heterodyne focal-plane arrays is nonetheless challenging.

6. "Backend" Spectrometers

In going from a single-element receiver to an array, the task of spectral elements is essentially multiplied by the number of elements in the array, although some aspects of the computing hardware may not be increased by a factor as large as $N_{element}$. All of the sub-millimeter heterodyne focal-plane arrays that have been used for astronomical observations have included an "array spectral processor:" a set of digital spectrometers that provides the required frequency resolution. The rapid progress in digital-signal-processing technology means that this part of the overall system is no longer the huge problem that it once was. A variety of approaches has been used in the spectrometers described in the references given in Table 1, including custom integrated circuits and, recently, field-programmable gate arrays (FPGAs). Depending to a degree on the environment in which they will be used, the 14 to 100 (or more, for currently-envisioned systems) spectrometers, each with the multi-GHz bandwidth required for sub-millimeter spectroscopy, do present some challenges.

While not part of the spectrometer system per se, an important issue for large systems is the signal transport from the receiver front end to the spectrometers. The traditional design for radio observatories has had the electronics located in a separate room, which can be in the base of the telescope, or in a separate building that can be close by or at some distance. In any case, sending the data over coaxial cables has been largely replaced by fiber-optic transmission systems. Even these are not inexpensive, and the fiber-optic cables themselves are costly. Their flexing due to telescope motion has been found to degrade the quality of spectral baselines. A promising technique is to digitize the output of each element right as part of the receiver itself, and to transmit information to the spectrometer (be it located near or far from the receiver) digitally.

The above suggests that the spectrometer system should be located as close to the receiver front end as possible. This is done in the upGREAT system on SOFIA [24, 25], for which the digital spectrometers are mounted in a rack that moves with the telescope, as does the receiver. This has proven to provide much better performance compared to what was achieved when the spectrometers were connected with flexible cables to the receiver, a deleterious effect that has been identified on other telescopes, as well.

The ability to locate the spectrometer system close to the receiver depends on its physical volume not being too large. Even with current FPGA technology, this is a challenge when considering arrays of ~ 100 elements. The problem of packing many FPGA-based spectrometers

close together is exacerbated by the challenge of dissipating the heat generated. A Virtex-7 FPGA-based 2048-channel FFT spectrometer dissipates at least 10 W of power. This is acceptable for ground-based systems, but packing such systems together in a rack is already problematic for aircraft operation, due to the lower air density on e.g. SOFIA. It would obviously be even more of a challenge for a space-based sub-millimeter instrument, where the total power dissipation of 1 kW for a 100-element array could be a show-stopper, in addition to the effort required to keep the circuitry from overheating.

One solution to this is to employ custom CMOS ASIC chips. These can be designed to include the digitizer, spectral processor, memory, and output interface circuitry. A major advantage is that the power consumption is far lower, since there are no transistors used to control the configuration of the processor itself. Of course, the price paid is that the system cannot be reconfigured: the functionality must be as desired in order to be of any use at all, and there is substantial up-front cost in this approach. A CMOS ASIC chip, offering comparable or superior performance to the FPGA-based system discussed above, could be implemented requiring less than 1 W of dc power [88-90]. This would allow a very compact unit to be placed close to the receiver, or even to be part of it, largely eliminating interface costs and offering superior performance from the rigid connection that would be enabled.

7. Sub-millimeter Heterodyne Focal-Plane Arrays Employed for Astronomical Observations

The title of this section is meant to indicate that we restrict ourselves to sub-millimeter heterodyne focal-plane arrays used on telescopes for astronomical observations. We extend the definition of sub-millimeter to include the 1.3 mm wavelength system described in [34]. In Table 1, we have compiled some of the key properties of the different heterodyne focal-plane arrays. Additional information on mm-wavelength heterodyne focal-plane arrays can be found in [1]. The variety of techniques used for the different functions indicates that there is no one best solution or standard design philosophy. The seven- and 14-element arrays were in hexagonal format, while the nine- and 2^n -element arrays had a square format.

The frequency range is not given for all arrays, as this was sometimes evolving or determined only by available local-oscillator sources. The Dual Band arrays, as suggested by the name, can operate simultaneously in two different, quite distinct frequency bands. Information about the telescopes where the arrays were/are employed can be found in the articles referenced.

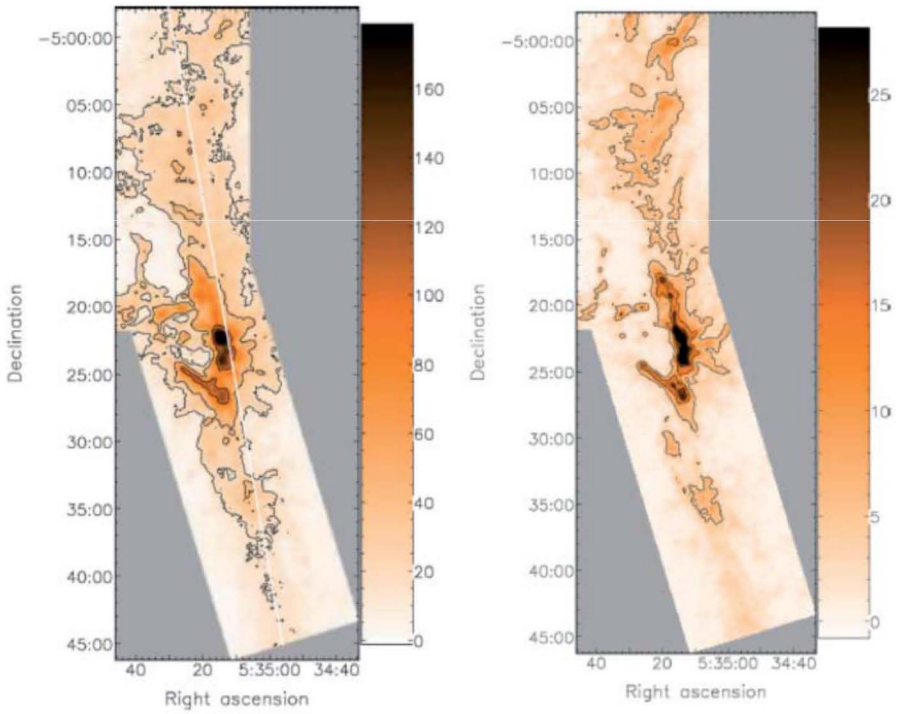

Figure 8. Images of the integrated intensity of the $J = 3 - 2$ transition of ^{13}CO and $C^{18}O$ in Orion [103], made with the 16-element HARP array [21]. The color bar on the right side of each image gives the integrated intensity in units of K-km/s. The two transitions were simultaneously observed with a velocity resolution of 0.05 km/s. The N-S extent of the images was 45 arcminutes, while the effective angular resolution was 17.3 arcseconds.

8. Summary, Conclusions, and Future Prospects

The first spectral line detected using a heterodyne system was the 345 GHz (870 μm) $J = 3-2$ transition of CO, observed in emission from Orion in 1977 [98] – unless you stretch the wavelength range to include the 230 GHz (1.3 mm) $J = 2-1$ transition first detected in interstellar space in 1973 [45]. Both of these early observations were made using InSb hot-electron-bolometer mixers [44]. These observations did confirm two critical points: (1) The emission from CO and other species is spatially extended on a scale of many arcminutes to degrees on the sky; (2) There is significant spectral structure in the line profiles that requires velocity resolution of a few km/s or higher ($R \geq 10^5$).

These two characteristics clearly established the need for sub-millimeter heterodyne focal-plane arrays to discern the structure of giant molecular clouds (a newly discovered phase of the interstellar medium), to determine their size, mass, and density, and to unravel their connection with star formation. Within a few years, the InSb mixers were superseded by Schottky barrier diode mixers that very rapidly were extended to operation throughout the sub-millimeter range, working from 200 GHz to 350 GHz [99], to 690 GHz [100], to 810 GHz [101], to 1900 GHz [102], and to 2500 GHz [103]. However, as discussed above, for the high sensitivity demanded by astronomical observations, Schottky barrier diodes (ambient temperature and cryogenically cooled) have in turn been replaced by superconductor-insulator-superconductor and hot-electron-bolometer mixers that while far more demanding in terms of operating temperature, are significantly more sensitive.

It was $\sim 20+$ years after the first heterodyne spectral-line detection that the first reference to a sub-millimeter heterodyne focal-plane array included in Table 1 appeared: the CHAMP array is therein described as "under development." During the intervening years, there have been great technological developments in all aspects of sub-millimeter receiver design, with extensive use of quasioptical components, superconductor-insulator-superconductor mixers, frequency-multiplied local oscillators, and a digital spectrometer system. All of this made the progression from single-element receivers to arrays practical, although they have remained complex engineering challenges.

To give one example of the results, Figure 8 includes images of the $J = 3-2$ transition of the carbon monoxide isotopologues ^{13}CO and $C^{18}O$ in Orion [104], made with the HARP array [23]. These lines are far weaker than the same transition of the common isotopologues ^{12}CO, but tell us much more about the actual column density of material in the region, as well as giving a picture of the cloud's kinematics: information that is obscured by the high optical depth of ^{12}CO. The (simultaneous) observation of these two lines (enabled by the digital backend spectrometer) required 34.2 hours of telescope time. The high sensitivity of the HARP elements suggests that with a single-element system, the time required would have been 16 times greater, or almost 550 hours. This illustrates both the impact of a heterodyne focal-plane array, and the obvious drive to construct even large arrays to enable high-angular-resolution velocity-resolved spectral imaging of large areas of the sky.

What can we expect in the next 20 years? The rapid evolution of sub-millimeter technology warns against excessive prognostication, but at least the following trends are clear:

1. A critical consideration for heterodyne focal-plane arrays is that the gain in time to map a given region decreases in proportion to the number of elements, but increases as the system temperature squared. Designers must thus increasingly look to minimize the quantity $T_{sys}^2 / N_{element}$. System designs will thus have to consider all factors that affect this quantity when choosing and optimizing their design.

2. The maturity of superconductor-insulator-superconductor and hot-electron-bolometer technology means that designing the circuits and fabricating the mixer elements for large heterodyne focal-plane arrays should be straightforward, and that yields should be relatively high.

3. The development of frequency-multiplied sources, complemented by the availability of quantum cascade lasers at the shorter sub-millimeter wavelength, means that providing the local oscillator for large arrays will be possible, but the optimum way to do this is not yet clear.

4. The development of lower-power IF amplifiers suggests that improved performance will be achieved in arrays by integrating at least the first few stages of IF gain with the mixers.

5. The ongoing development of digital signal processing capability will continue to reduce the cost of the spectrometer system. Tighter integration of the spectrometer and the receiver would improve performance and reduce costs, but this depends on the availability of lower-power processing, possibly by taking advantage of CMOS ASIC systems.

Some things that are not so clear are:

1. Will new materials, such as MgB_2 MgB_2 for sub-millimeter hot-electron-bolometer mixers, enable operation at higher temperatures, thus easing the cryogenic design for large arrays, as well as increasing the instantaneous bandwidth?

2. Will MMIC amplifiers become competitive with superconductor-insulator-superconductor mixers at frequencies above 100 GHz, bringing some of the impressive results that have been demonstrated at longer wavelengths?

3. Will the impetus continue to develop sub-millimeter heterodyne focal-plane arrays for operation above the Earth's atmosphere, where system noise temperature improvements are directly reflected in gains in system sensitivity, and where "`blocked" spectral lines can be studied?

4. Telescope time is expensive, and if the scientific interest in spectral-line imaging continues, large HPFAs are financially justified. One can hope that there will continue to be airplane, balloon, and space-borne observatories on which such arrays can be used, and that the development and deployment of such arrays on these platforms is in every way justified.

Watching the ongoing development of heterodyne focal-plane arrays in the years ahead will be exciting from the point of view of technological developments, as well as providing exciting and beautiful new scientific results.

9. Acknowledgements

I am very pleased to have this chance to acknowledge the support and encouragement I received over many years from my very good friend and colleague, Gianni Tofani. Gianni was invariably enthusiastic about astronomical discoveries, new observational facilities, and new technology. He worked for years to get the Sardinia Radio Telescope built, and served with me on the Advisory Committee in the early years of the Large Millimeter Telescope in Mexico. He gave a great deal to a variety of people and projects, but was himself very modest about his contributions. Gianni was my sponsor and gracious host during two sabbatical visits to Florence. He enjoyed so much in life with his wife, Annamaria, that it remains painful to think that he is no longer with us. I am happy to recognize the assistance received from my colleagues at JPL and elsewhere, including Jonathan Kawamura, Jose Siles, Adrian Tang, Urs Graf, Chris Groppi, and Richard Hills. These generous experts all shared their work and ideas, and answered many questions. Richard Hills was particularly generous in his careful reading of this contribution, and making many suggestions that improved it. This work was carried out at the Jet Propulsion Laboratory, which is operated for NASA by the California Institute of Technology.

10. References

1. C. E. Groppi and J. H. Kawamura, "Coherent Detector Arrays for Terahertz Astrophysics Applications," *IEEE Transactions on Terahertz Science and Technology*, **1**, September 2011, pp. 85-96.

2. U. U. Graf, C. E. Honingh, K. Jacobs, and J. Stutzki, "Terahertz Heterodyne Array Receivers for Astronomy," *Journal Infrared Millimeterwave and Terahertz Waves*, **36**, 2015, pp. 896-921.

3. M. Born and E. Wolf, *Principles of Optics*, Oxford, Pergamon, 1959, p. 395.

4. E. Hecht and A. Zajac, Optics, Reading, Addison-Wesley, 1979, p. 350.

5. J. D. Kraus, *Antennas, Second Edition*, New York, McGraw-Hill, 1988, p. 410.

6. P. F. Goldsmith, "Radio Telescopes and Measurements at Radio Wavelengths," in *Single-Dish Radio Astronomy: Techniques and Applications*, ASP Conference Series, Vol. 278, 2002.

7. J. W. Lamb, "Quasioptical Coupling of Gaussian Beam Systems to Large Cassegrain Antennas," *International Journal of Infrared and Millimeter Waves*, **7**, 10, 1986, pp. 1511-1536.

8. P. F. Goldsmith, *Quasioptical Systems*, New York, IEEE Press/Chapman & Hall, 1998, Chapter 6.

9. R. J. Wylde, "Millimetre Wave Gaussian Beam-Mode Optics and Corrugated Feed Horns," *Microwaves Optics and Antennas*, **131**, August 1984, pp. 258-282.

10. A. Gonzalez, K. Kaneko, T. Kojima, S. Asayama, and Y. Uzawa, "Terahertz Corrugated Horns (1.25-1.57 GHz): Design, Gaussian Modeling, and Measurements," IEEE Transactions *on Terahertz Science and Technology*," **7**, January 2017, pp. 42-52.

11. J. F. Johansson and N. D. Whyborn, "The Diagonal Horn as a Sub-Millimeter Wave Antenna," *IEEE Transactions on Antennas and Propagation*, **AP-40**, May 1982, pp. 795-800.

12. C. Granet, G. L. James, R. Bolton, and G. Moorey, "A Smooth-Walled Spline-Profile Horn as an Alternative to the Corrugated Horn for Wide Band Millimeter-Wave Applications," *IEEE Transactions on Antennas and Propagation*, **52**, March 2004, pp. 848-854.

13. L. Zeng, C. L. Bennett, D. T. Chuss, and E. J. Wollack, "A Low Cross-Polarization Smooth-Walled Horn with Improved Bandwidth," *IEEE Transactions on Antennas and Propagation*, **58**, April 2010, pp. 1383-1387.

14. N. Chahat, T. J. Reck, C. Jung-Kubiak, T. Nugyen, et al., "1.9-THz Multiflare Angle Horn Optimization for Space Instrumentation," *IEEE Transactions on Terahertz Science and Technology*," **5**, November 2015, pp. 914-920.

15. L. Chen, C. E. Tong, and P. K. Grimes, "Experimental Verification of the Fundamental Gaussian Beam Properties of Smooth-Walled Feedhorns, "*IEEE Transactions on Terahertz Science and Technology*," **6**, January 2016, pp. 163-168.

16. H. Kogelnik and T. Li, "Laser Beams and Resonators," *Proceedings of the IEEE*," **54**, October 1966, pp. 1312-1329.

17. A. E. Siegman, *Lasers*, Mill Valley, University Science Books, 1986, Chapter 17.

18. P. F. Goldsmith, "Quasi-Optical Techniques at Millimeter and Submillimeter Wavelengths," in *Infrared and Millimeter Waves*, **6**, New York, Academic Press, 1982.

19. P. F. Goldsmith, "Radiation Patterns of Circular Apertures with Gaussian Illumination," *International Journal of Infrared and Millimeter Waves*, **8**, 7, 1987, pp. 771-782.

20. C. Kasemann, R. Güsten, S. Heyminck, B. Klein, et al., "CHAMP$^+$: A Powerful Array Receiver for APEX," Millimeter and Submillimeter Detectors and Instrumentation for Astronomy III, *Proceedings of SPIE*, **6275**, 2006, pp. 62750N-1-62750N-12.

21. C. Risacher, R. Güsten, J. Stutzki, H.-W. Hübers, et al., "First Supra-THz Heterodyne Array Receivers for Astronomy with the SOFIA Observatory," *IEEE Transactions on Terahertz Science and Technology*, **6**, March 2016, pp. 199-211.

22. C. Risacher, R. Güsten, Jürgen Stutzki, H.-W. Hübers, et al., "The upGREAT 1.9 THz Multi-Pixel High Resolution Spectrometer for the SOFIA Observatory," *Astronomy and Astrophysics*, **9**, 595, 2016, A34.

23. J. V. Buckle, R. E. Hills, H. Smith, W. R. F. Dent, et al., "HARP/ACIS: A Submillimetre Spectral Imaging System on the James Clerk Maxwell Telescope," *Monthly Notices of the Royal Astronomical Society*, **399**, 2009, pp. 1026-1043.

24. C. Groppi, C. Walker, C. Kulesa, D. Golish, et al., "SuperCam: a 64 Pixel Heterodyne Imaging Spectrometer," Millimeter and Submillimeter Detectors and Instrumentation for Astronomy IV, *Proceedings of SPIE*, **7020**, 2008, pp. 702011-1-702011-8.

25. C. Groppi, C. Walker, C. Kulesa, D. Golish, et al., "Test and Integration Results from SuperCam: a 64-Pixel Array Receiver for the 350 GHz Atmospheric Window," Millimeter, Submillimeter, and Far-Infrared Detectors and Instrumentation for Astronomy V, *Proceedings of SPIE*, **7741**, 2010, pp. 77410X-1-77410X-12.

26. A. Krabbe, "The SOFIA Telescope," Airborne Telescope Systems, *Proceedings of SPIE*, **4014**, 2000, pp. 276-281.

27. N. R. Erickson, R. M. Grosslein, R. B. Erickson, and S. Weinreb, "A Cryogenic Focal Plane Array for 85-115 GHz Using MMIC Preamplifiers," *IEEE Transactions on Microwave Theory and Techniques*, **47**, December 1999, pp. 2212-2219.

28. J. Leech, B. K. Tan, G. Yassin, P. Kittara, and S. Wangsuya, Experimental Investigation of a Low-Cost, High Performance Focal-Plane Horn Array," *IEEE Transactions on Terahertz Science and Technology*, **2**, January 2012, pp. 61-70.

29. J. Kawamura, J. Kloosterman, J. Siles, F. Boussaha, et al., "Development of a 16-pixel Monolithic 1.9 THz Waveguide Superconducting Hot-Electron Bolometer Mixer," ISSTT Conference, Cologne, Germany, 2017.

30. J. Kawamura, private communication.

31. G. Rebeiz, "Millimeter-Wave and Terahertz Integrated Circuit Antennas," *IEEE Proceedings*, **80**, December 1992, pp. 1748-1770.

32. N. Llombart, G. Chattopadhyay, A. Skalare, and I. Mehdi, " Novel Terahertz Antenna Based on a Silicon Lens Fed by a Leaky Wave Enhanced Waveguide," *IEEE Transactions on Antennas and Propagation*, **59,** June 2011, pp. 2160-2168.

33. N. Llombart, C. Lee, M. Alonso-delPino, G. Chattopadhyay, et al., "Silicon Micromachined Lens Antenna for THz Integrated Heterodyne Arrays," *IEEE Transactions on Terahertz Science and Technology*, **3**, September 2013, pp. 515-523.

34. K.-F. Schuster, C. Boucher, W. Brunswig, M. Carter, et al., "A 230 GHz Heterodyne Receiver Array for the IRAM 30 m Telescope," *Astronomy and Astrophysics*, **423**, 2004, pp. 1171-1177.

35. N. R. Erickson, P. Goldsmith, G. Novak, R. Grosslein, et al., "A 15 Element Focal Plane Array for 100 GHz." *IEEE Transactions on Microwave Theory and Techniques*, **40**, January 1992, pp. 1-11.

36. J. R. Tucker and M. J. Feldman, "Quantum Detection at Millimeter Wavelengths," *Reviews of Modern Physics*, **57**, October 1985, pp. 1055-1113.

37. R. Blundell, R. E. Miller, and K.H. Gundlach, "Understanding Noise in SIS Receivers," *International Journal of Infrared and Millimeter Waves*, **13**, 1992, pp. 3-14.

38. C. E. Honingh, S. Haas, D. Hottgenroth, K. Jacobs, and J. Stutzki, "Low Noise Broadband Fixed Tuned SIS Waveguide Mixers at 660 GHz and 800 GHz," *IEEE Transactions on Applied Superconductivity*, **7**, June 1997, pp. 2582-2586.

39. J. W. Kooi, R. A. Chamberlin, R. Monje, A. Kovács, et al., "Performance of the Caltech Submillimeter Observatory Dual-Color 180-720 GHz Balanced SIS Receivers," *IEEE Transactions on Terahertz Science and Technology*, **4**, March 2014, pp. 149-164.

40. A. R. Kerr, S.-K. Pan, S. M. X. Claude, P. Dindo, et al.," Development of the ALMA Band-3 and Band-6 Sideband-Separating SIS Mixers," *IEEE Transactions on Terahertz Science and Technology*, **4**, March 2014, pp. 201-212.

41. Th. de Graauw, F. P. Helmich, T. G. Phillips, J. Stutzki, et al., "The *Herschel*-Heterodyne Instrument for the Far-Infrared (HIFI)," *Astronomy and Astrophysics*, **518**, 210, pp. 39-45.

42. K. Sunada, C. Yamaguchi, N. Nakai, K. Sorai, et al. "BEARS – SIS 25-Beam Array Receiver System for the NRO 45-m Telescope," *Proceedings of SPIE*, **4015**, 2000, pp. 237-246.

43. K.-F. Schuster, C. Boucher, W. Brunswig, M. Carter, et al., "A 230 GHz Heterodyne Receiver Array for the IRAM 30 m Telescope," *Astronomy and Astrophysics*, **423**, 2004, pp. 1171-1177.

44. T. G. Phillips and K. B. Jefferts, "A Low Temperature Bolometer Heterodyne Receiver for Millimeter Wave Astronomy," *Rev. Sci. Instruments*, **44**, August 1973, pp. 1009-1014.

45. T. G. Phillips, K. B. Jefferts, and P. G. Wannier, "Observation of the J = 2 to J = 1 Transition of Interstellar CO at 1.3 Millimeters," *The Astrophysical Journal*, **186**, November 1973, pp. L19-L22.

46. T. G. Phillips, P. J. Huggins, T. B. H. Kuiper, and R. E. Miller, "Detection of the 610 Micron (492 GHz) Line of Interstellar Atomic Carbon," *The Astrophysical Journal*, **238**, June 1980, pp. L103-L106.

47. C. R. Predmore, A. V. Räisänen, N. R. Ericson, P. F. Goldsmith, and J. L. R. Marrero, "A Broad-Band Ultra-Low-Noise Schottky Diode Mixer Receiver from 80 to 115 GHz," *IEEE Transactions on Microwave Theory and Techniques*, **MTT-32**, May 1984, pp. 498-507.

48. G. N. Gol'tsman, A. D. Semenov, Y. P. Gousev, M. A. Zorin, et al., "Sensitive Picosecond NbN Detector for Radiation from Millimetre Wavelengths to Visible Light," *Superconducting Science and Technology*, **4**, 1991, pp. 453-456.

49. E. M. Gershenzon, G. N. Gol'tsman, I. G. Gogidze, Y. P. Gusev, et al., "Millimeter and Submillimeter Range Mixer Based on Electronic Heating of Superconducting Films in the Resistive State," *Soviet Physics – Superconductivity*, **3**, 1991, pp. 1582-1590.

50. D. E. Prober, "Superconducting Terahertz Mixer Using a Transition-Edge Microbolometer," *Applied Physics Letters*, **62**, April 1993, pp. 2119-2121.

51. H. Ekström, B. S. Karasik, E. L. Kollberg, and K. S. Yngvesson, "Conversion Gain and Noise of Niobium Superconducting Hot-Electron-Mixers," *IEEE Transactions of Microwave Theory and Techniques*, **43,** April 1995, pp. 938-947.

52. A. D. Semenov, H.-W. Hübers, J. Schubert, G. N. Gol'tsman, et al., "Design and Performance of the Lattice-Cooled Hot-Electron Terahertz Mixer," *Journal of Applied Physics*, **88**, December 2000, pp. 6758-6767.

53. J. Kawamura, R. Blundell, C.-Y. Tong, D. C. Papa, T. R. Hunter, et al., "Superconductive Hot-Electron-Bolometer Mixer Receiver for 800-GHz Operation," *IEEE Transactions on Microwave Theory and Techniques*, **48**, April 2000, pp. 683-689.

54. L. Jiang, S. Shiba, K. Shimbo, N. Sakai, et al.," Development of THz Waveguide NbTiN HEB Mixers," *IEEE Transactions on Applied Superconductivity*, **19**, June 2009, pp. 301-304.

55. W. Zhang, P. Khosropanah, J. R. Gao, B. Banasai, et al., " Noise Temperature and Beam Pattern of an NbN Hot Electron Bolometer Mixer at 5.25 THz," *Journal of Applied Physics*, **108**, 2010, pp. 093102-1093102-7.

56. J.L. Kloosterman, D.J. Hayton, Y. Ren, T. Y. Kao, et al., "Hot Electron Bolometer Heterodyne Receiver With a 4.7-THz Quantum Cascade Laser as a Local Oscillator," *Applied Physics Letters*, **102**, 2013, pp. 011123-1-011123-4.

57. D. Büchel, P. Pütz, K. Jacobs, M. Schultz, et al., "4.7-THz Superconducting Hot Electron Bolometer Waveguide Mixer," *IEEE Transactions on Terahertz Science and Technology*, **5**, March 2015, p. 207-214.

58. S. Cherednichenko, V. Drakinskiy, K. Ueda, and M Naito, "Terahertz Mixing in MgB_2 Microbolometers," *Applied Physics Letters*, **90**, 2007, pp. 023507-1-023507-3.

59. S. Bevilacqua, S. Cherednichenko, V. Drakinskiy, J. Stake, et al., "Low Noise MgB_2 Terahertz Hot-Electron Bolometer Mixers," *Applied Physics Letters*, **100**, 2012, pp. 033504-1-033504-3.

60. SE. Novoselov and S. Cherednichenko, "Low Noise Terahertz MgB_2 Hot-Electron Bolometer Mixers With an 11 GHz Bandwidth," *Applied Physics Letters*, **110**, 2017, pp. 032601-1-032601-5.

61. D. Cunnane, J. H. Kawamura, M. A. Wolak, N. Acharya, et al., "Optimization of Parameters of MgB2 Hot-Electron Bolometers," *IEEE Transactions on Applied Superconductivity*, **27**, June 2017, p. 2300405.

62. S. Cherednichenko, V. Drakinskiy, T. Berg, P. Khosropanah, and E. Kollberg, "Hot-Electron Bolometer Terahertz Mixers for the Herschel Space Observatory," *Review of Scientific Instruments*, **79**, 2008, pp. 034501-1-034501-10.

63. D. Cuadrado-Calle, D. George, G.A., Fuller, K. Cleary, et al., "Broadband MMIC LNAs for ALMA Band 2+3 with Noise Temperature Below 28 K," *IEEE Transactions on Microwave Theory and Techniques*, **65**, May 2017, pp. 1589-1597.

64. P. Kangaslahti, P., K. Cleary, J. Kooi, L. Samoska, et al., "Sub-20-K Noise Temperature LNA for 67-90 Frequency Band," Proceedings of the IEEE International Microwave Symposium, Honolulu, HI, June, 2017, pp. 1-4.

65. M. Sieth, K. Devaraj, P. Voll, S. Church, et al., "Argus: A 16-Pixel Millimeter-Wave Spectrometer for the Green Bank Telescope," *Proceedings of SPIE*, **9153**, 2014, pp. 91530P-1-91530P-12.

66. K. M. K. H. Leong, X Mei, W. Yoshida, P.-H. Liu, et al., "A 0.85 THz Low Noise Amplifier Using InP HEMT Transistors," *IEEE Microwave and Wireless Components Letters*, **25**, June 2015, pp. 397-309.

67. X. Mei, W. Yoshida, M. Langer, J. Lee, et al., "First Demonstration of Amplification at 1 THz Using 25-nm InP High Electron Mobility Transistor Process," *IEEE Electron Device Letters*, **36**, April 2015, pp. 327-329.

68. B. S. Williams, "Terahertz Quantum-Cascade Lasers," *Nature Photonics*, **1**, September 2007, pp. 517-525.

69. C. Ling, T. Liu, and Q. J. Wang, "Recent Developments of Terahertz Quantum Cascade Lasers," *IEEE Journal of Selected Topics in Quantum Electronics*, **23**, July/August 2017, pp. 1200118.

70. Y. Ren, D. N. Hovenier, M. Cui, D. J. Hayton, et al., "Frequency locking of a Single-Mode 3.5-THz Quantum Cascade Lasers Using a Gas Cell," *Applied Physics Letters*, **100**, 2012, 041111.

71. D. Rabanus, U. U. Graf, M. Philipp, O. Ricken, et al., "Phase Locking of a 1.5 Terahertz Quantum Cascade Laser and Use as a Local Oscillator in a Heterodyne HEB Receiver," *Optics Express* **17**, 2 February 2009, 1159; P. Khosropanah, A. Baryshev, W. Zhang, W. Jellema, et al., "Phase Locking of a 2.7 THz Quantum Cascade Laser to a Microwave Reference," *Optics Letters*, **34**, October 1, 2009, pp. 2958-2960.

72. H.-W. Hübers, S. G. Pavlov, G. Semenov, R. Köhler, et al. "Terahertz Quantum Cascade Laser as Local Oscillator in a Heterodyne Receiver," *Optics Express*, **13**, 2005, pp. 5890-5896.

73. J. Kloosterman, D. J. Hayton, Y. Ren, T. Y. Kao, et al., "Hot Electron Bolometer Heterodyne Receiver with a 4.7 THz Quantum Cascade Laser as a Local Oscillator," *Applied Physics Letters*, **102**, 2013, 011123.

74. A. Maestrini, J. S. Ward, J. J. Gill, C. Lee, et al., "A Frequency-Multiplied Source with More than 1 mW of Power Across the 840-900 GHz Band," *IEEE Transactions on Microwave Theory and Techniques*, **58**, July 2010, pp. 1925-1932.

75. G. Chattopadhyay, E. Schlecht, J. S. Ward, J. J. Gill, et al., "An All-Solid-State Broad-Band Frequency Multiplier Chain at 1500 GHz," *IEEE Transactions on Microwave Theory and Techniques*, **52**, May 2004, pp. 1538-1547.

76. J. V. Siles, R. H. Lin, C. Lee, E. Schlecht, et al., "Development of High-Power Multi-Pixel LO Sources at 1.47 THz and 1.9 THz for Astrophysics: Present and Future," Proceedings of 26th International Symposium on Space Terahertz Technology, March 2015, T1-3.

77. F. Boussaha, J. Kawamura, J. Stern, and C. Jung-Kubiak, "2.7 THz Balanced Waveguide HEB Mixer," *IEEE Transactions on Terahertz Science and Technology*, **4**, September 2014, pp. 545-551.

78. U. U. Graf and S. Heyminck, "Fourier Gratings as Submillimeter Beam Splitters," *IEEE Transactions on Antennas and Propagation*, **49**, April 2001, pp. 542-546.

79. B. Mirzaei, J. R. G. Silva, Y. C. Luo, X. X. Liu, et al. "Efficiency of Multi-Beam Fourier Phase Gratings at 1.4 THz," *Optics Express*, **25**, 20 March 2017, pp. 6581-6588.

80. S. Heyminck and U. U. Graf, "Array-Receiver LO Unit Using Collimating Fourier-Gratings," Proceedings 12th International Symposium on Space Terahertz Technology," 2001, pp. 563-570.

81. M. Kotiranta, C. Lenz, T. Klein, V. Krozer, and H. J. Wunsch, "Characterization of Imperfections in a Martin-Puplett Interferometer Using Ray Tracing," *Journal of Infrared Millimeter, and Terahertz Waves*, **33**, 2012, pp. 1138-1148.

82. S. Claude, "Sideband-Separating SIS Mixer for ALMA Band 7, 275-370 GHz," Proceedings 14th International Symposium on Space Terahertz Technology, 2003, pp. 41-51.

83. F. P. Mena, J. W. Kooi, A. M. Baryshev, C. F. J. Lodewijk, et al. "Design and Performance of a 600-720 GHz Sideband Separating Receiver Using AlO_x and AlN SIS Junctions," *IEEE Transactions on Microwave Theory and Techniques*, **59**, January 2011, pp. 166-177.

84. R. Rodríguez, R. Finger, F. P. Mena, N. Reyes, et al., "A Sideband-Separating Receiver with a Calibrated Digital IF-Hybrid Spectrometer for the Millimeter Band," *Publications of the Astronomical Society of the Pacific*, **125**, April 2014, pp. 380-385.

85. D. Kester, R. Higgins, and D. Teyssier, "Derivation of Sideband Gain Ratio for Herschel/HIFI," *Astronomy and Astrophysics*, **599**, 2017, pp. A115-1 – A115-13.

86. U. U. Graf. "A Compact Beam Measurement Setup," *Journal Infrared Millimeter and Terahertz Waves*, **37**, 2016, pp. 770-775.

87. S. Montazeri, W.-T. Wong, A. H. Coskun, and J. C. Bardin, "Ultra-Low-Power Cryogenic SiGe Low-Noise Amplifiers: Theory and Demonstration, *IEEE Transactions on Microwave Theory and Techniques*, **64**, January 2016, pp. 178-187.

88. A. Hsiao, A. Tang, Y. Kim, B. Drouin, et al., "A 2.2 GS/s 188 mW Spectrometer Processor in 65nm CMOS for Supporting THz Planetary Instruments," Proc. 2015 IEEE Custom Integrated Circuits Conference.

89. A. Amara, F. Amiel, and T. Ea, "FPGA vs. ASIC for Low Power Applications," *Microelectronics Journal*, **27**, pp. 669-677.

90. A. Tang, private communication

91. R. Güsten, G. Ediss, F. Gueth, K. Gundlach, et al., "CHAMP – The Carbon Heterodyne Array of the MPIfR," *Proceedings of SPIE*, **3357**, March 1998, pp. 167-177.

92. C. Groppi, C. Walker, A. Hungerford, C. Kulesa, et al., "Pole STAR: An 810 GHz Array Receiver for AST/RO," *ASP Conference Proceedings*, **217**, 2000, pp. 48-49.

93. C. Walker, C. Groppi, D. Golish, C. Kulesa, et al., "PoleStar: An 810 GHz Array Receiver for AST/RO," Proceedings 12th International Symposium on Space Terahertz Technology, 2001, pp. 540-551.

94. U. U. Graf, S. Heyminck, E. A. Michael, S. Stanko, et al., "SMART: The KOSMA Sub-Millimeter Array Receiver for Two Frequencies," Proc. 13th International Symposium on Space Terahertz Technology, March 2002, pp. 143-151.

95. C. E. Groppi, C. K. Walker, C. Kulesa, D. Golish, et al., "Desert STAR: A 7 Pixel 345 GHz Heterodyne Array Receiver for the Heinrich Hertz Telescope," *Proceedings of SPIE*, **4855**, 2003, pp. 330-337.

96. C. E. Groppi, C. K. Walker, C. Kulesa, D. Golish, et al., "First Results from Desert STAR: A 7 Pixel 345 GHz Heterodyne Array Receiver for the Heinrich Hertz Telescope," *Proceedings of SPIE*, **5498**, 2004, pp. 290-298.

97. 97. H. Smith, J. Buckle, R. Hills, G. Bell, et al. "HARP: a Submillimetre Heterodyne Array Receiver Operating on the James Clerk Maxwell Telescope," *Proc. of SPIE*, **7020**, 2008, pp. 70200Z-1 - 70200Z-15.

98. T. G. Phillips, P. J. Huggins, G. Neugebauer, and M. W. Werner, "Detection of Submillimeter (870 μm) CO Emission from the Orion Molecular Cloud," *The Astrophysical Journal*, **217**, November 1 1977, pp. L161-L164.

99. N. R. Ericson, "A 200-350 GHz Heterodyne Receiver," *IEEE Transactions on Microwave Theory and Techniques*, **MTT-29**, June 1981, pp. 557-561.

100. P. F. Goldsmith, N. R. Ericson, H. R. Fetterman, B. J. Clifton, et al., "Detection of the J = 6-5 Transition of Carbon Monoxide," *The Astrophysical Journal*, **243**, January 15 1981, pp. L79-L82.

101. D. T. Jaffe, A. I. Harris, M. Silber, R. Genzel, and A. L. Betz, " Detection of the 370 Micron $^3P_2$-$^3P_1$ Fine-Structure line of [CI]," *The Astrophysical Journal*, **290**, 1985 March 15, pp. L59-L62.

102. R. T. Boreiko, A. L. Betz, and J. Zmuidzinas, "Heterodyne Spectroscopy of the 158 Micron C II Line in M42," *The Astrophysical Journal*, **325**, 1988 February 15, pp. L47-L51.

103. A. L. Betz and R. T. Boreiko, "Reversed Far-Infrared Line Emission from OH in Orion," *The Astrophysical Journal,* **346**, 1989 November 15, pp. L101-L104.

104. J. V. Buckle, C. J. Davis, J. Di Francesco, S. F. Graves, et al., "The JCMT Legacy Survey of the Gould Belt: Mapping ^{13}CO and $C^{18}O$ in Orion A," *Monthly Notices of the Royal Astronomical Society*, **422**, 2012, 521-541.